Journal of Asian Earth Sciences 44 (2012) 136–148

Contents lists available at ScienceDirect

Journal of Asian Earth Sciences

journal homepage: www.elsevier.com/locate/jseaes

Cenozoic evolution of the Pamir plateau based on stratigraphy, zircon provenance, and stable isotopes of foreland basin sediments at Oytag (Wuyitake) in the Tarim Basin (west China)

John Bershaw [a,*], Carmala N. Garzione [a], Lindsay Schoenbohm [b], George Gehrels [c], Li Tao [d]

[a] Department of Earth and Environmental Sciences, University of Rochester, 227 Hutchison Hall, Rochester, NY 14627, USA
[b] Department of Chemical and Physical Sciences, University of Toronto Mississauga, 3359 Mississauga Road N., Mississauga, Ontario, Canada L5L 1C6
[c] Department of Geosciences, University of Arizona, Gould-Simpson Blgd. #77, 1040 E 4th St., Tucson, AZ 85721, USA
[d] State Key Laboratory of Earthquake Dynamics, Institute of Geology, China Earthquake Administration, Beijing, China

ARTICLE INFO

Article history:
Received 31 August 2010
Received in revised form 16 March 2011
Accepted 18 April 2011
Available online 29 April 2011

Keywords:
Provenance
Pamir plateau
Himalaya
Tibetan plateau
Tarim Basin
U–Pb ages
Detrital zircons
Stable isotopes
Paleoaltimetry
Paleoclimate
Stratigraphy

ABSTRACT

The Pamir salient is the western expression of mountain growth related to Indo-Eurasian convergence. Though a rough framework has emerged describing the tectonic evolution of the Pamir, detailed knowledge of the spatial and temporal evolution of Cenozoic deformation is necessary to determine how strain progressed through the orogenic belt. Here we present new stratigraphic, zircon provenance, and stable isotope data from Jurassic to Miocene strata along the Pamir's northeastern margin near the town of Oytag (Wuyitake) in the Tarim Basin (west China). Prominent ~40 Ma peaks in Oligocene to early Miocene detrital zircon grains record the erosion of an Eocene belt of shoshonitic rocks in the central to southeastern Pamir. This is roughly coincident with an ~4‰ shift in the oxygen isotopic composition ($\delta^{18}O$) of carbonates during the Eocene and/or Oligocene (from an average of −8.7‰ to −12.6‰), suggesting a reorganization of atmospheric circulation during that time. This could have been caused by uplift of Tarim Basin-bounding ranges and/or retreat of the Paratethys Sea.

A subsequent change from Eocene to Jurassic aged detrital zircon grains in the early to middle Miocene indicates provenance shifted from source rocks in the central and/or SE Pamir to the hanging wall of the Main Pamir Thrust (MPT), coincident with prograding facies at that time. This suggests deformation progressed outward toward the northeast margin of the Pamir plateau in the early to middle Miocene. Our results corroborate outward advancement of Himalayan deformation, affecting all margins of the Tarim Basin by the middle Miocene.

1. Introduction

The Cenozoic evolution of the Pamir plateau, like the Tibetan plateau, is tied to Indo-Eurasian convergence (Fig. 1). At an average elevation in excess of 4 km, the Pamir plateau impedes westerly atmospheric flow, contributing to the arid climate presently observed in the western Tarim Basin. A detailed history of plateau deformation is necessary to understand when the Pamir became a significant topographic barrier and how crustal heterogeneities have affected the style and spatial distribution of deformation through time. Better constraints on the timing of Pamir deformation will also provide insight into its genetic relationship to the neighboring Tibetan plateau and the Tian Shan.

The Pamir is composed of along-strike equivalents of Himalayan and Tibetan plateau tectonic terranes that accreted onto Eurasia during the Paleozoic and Mesozoic (Burtman and Molnar, 1993; Schwab et al., 2004; Robinson, 2009). Significant contraction during the Cenozoic has resulted in thrust and strike-slip faulting that generally follows the arcuate trend of the Pamir salient (Figs. 1 and 2). Thrusting of the Pamir's leading edge over the Tian Shan to the north along the Main Pamir Thrust (MPT) continues today (Coutand et al., 2002), accommodating ~10% of the present convergence between India and Eurasia (Arrowsmith and Strecker, 1999).

The data presented in this study come from the Pamir's northeastern margin, an area where major thrust, normal, and strike-slip faults coexist. The direction, timing, and magnitude of offset along many of these faults is still not well constrained. Temporal changes in the provenance of detrital zircons within foreland basin sedimentary rocks can be used to infer significant shifts in the assemblage of source terranes from which sediments are derived (e.g. Gehrels and Dickinson, 1995; Bruguier et al., 1997; Ireland et al., 1998). Here we present detrital zircon data from a previously measured stratigraphic section of Mesozoic sedimentary rocks (e.g. Sobel, 1995) and newly measured and described Cenozoic rocks on

* Corresponding author. Tel.: +1 585 275 5713; fax: +1 585 244 5689.
E-mail address: jbershaw@gmail.edu (J. Bershaw).

1367-9120/$ - see front matter © 2011 Elsevier Ltd. All rights reserved.
doi:10.1016/j.jseaes.2011.04.020

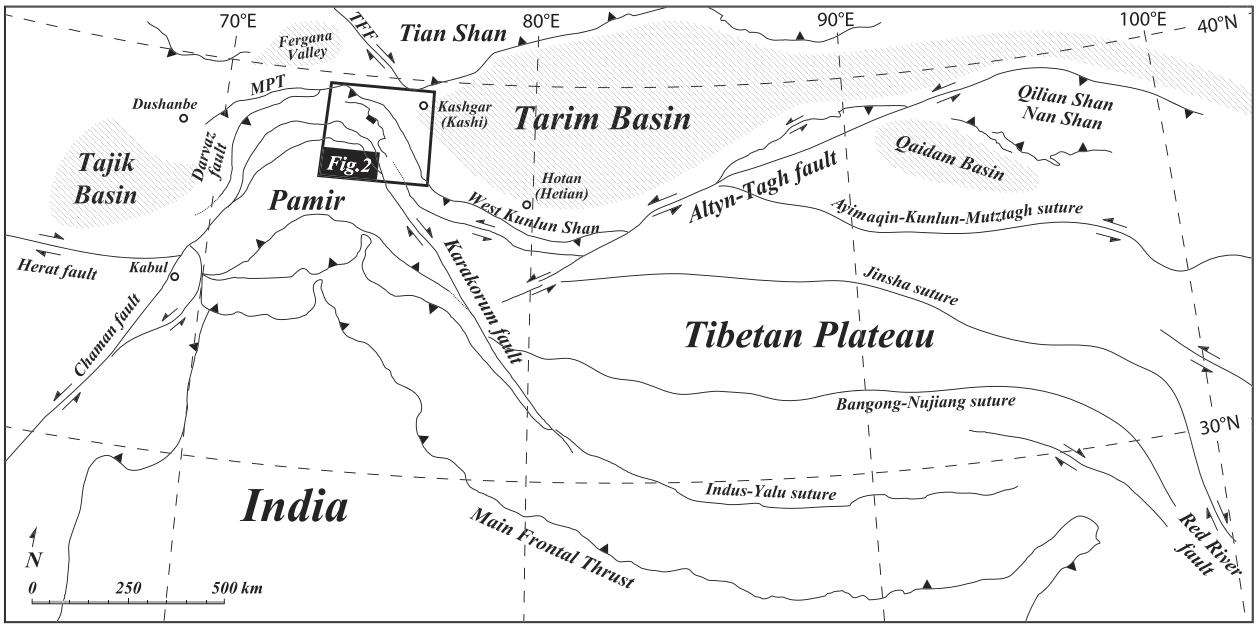

Fig. 1. Map of Asia showing the Pamir relative to Tibet and the Himalayan front with locations of major basins (cross-hatched) and regional-scale structures. TFF = Talas-Fergana fault. MPT = Main Pamir Thrust fault. Figure adapted from Burtman (2000), Cowgill (2010), Robinson et al. (2007), Schwab et al. (2004) and Yin et al. (2002).

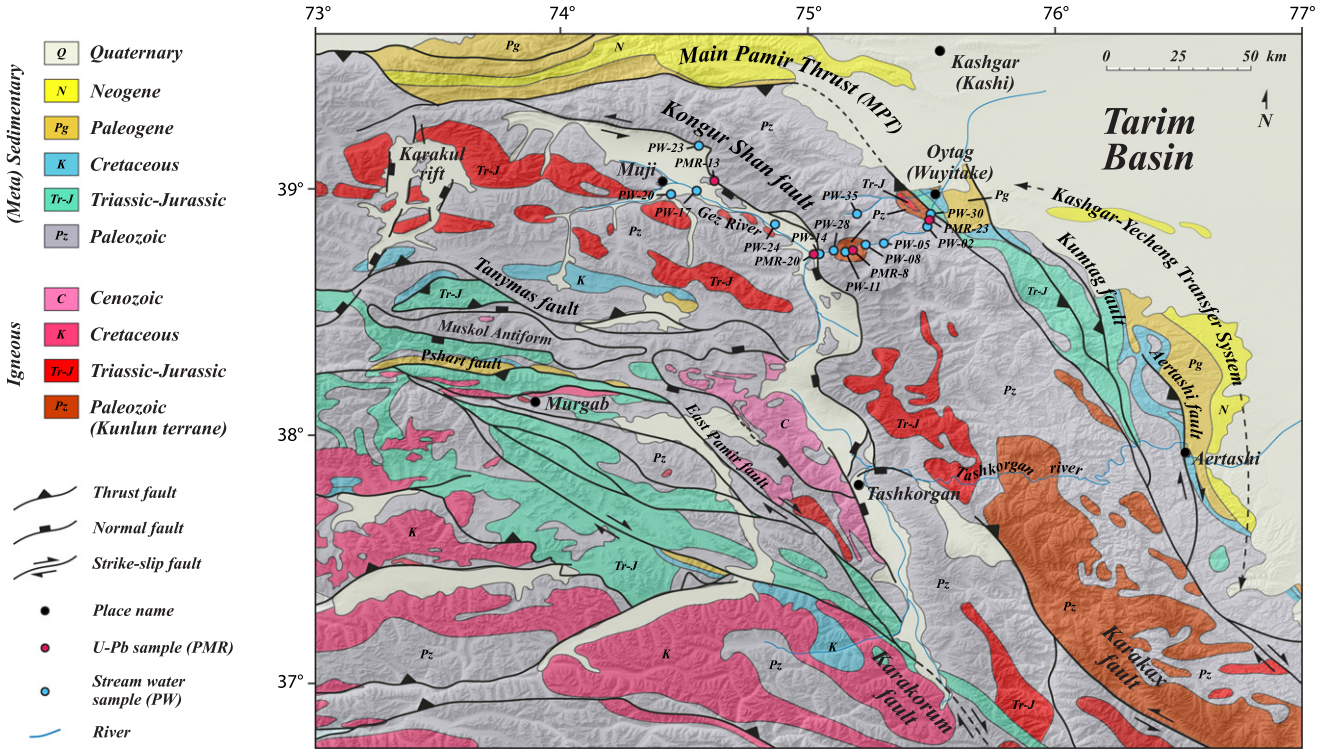

Fig. 2. Map of eastern Pamir including major geologic units overlain on shaded relief topography derived from satellite data (SRTM from http://srtm.csi.cgiar.org/). Location shown in Fig. 1. U–Pb sample locations (red dots with prefix "PMR-") represent source terranes. All other U–Pb samples were collected from the stratigraphic section near Oytag (Fig. DR1). Surface water samples were collected from tributaries to the Gez River (blue dots with prefix "PW-"). Coordinates for all samples are presented in Tables 1, 2, and Table DR1. Place names are in Uygur with Chinese Pinyin in parentheses. Figure adapted from Cowgill (2010), Robinson et al. (2007), Schwab et al. (2004), and Sobel and Dumitru (1997). (For interpretation of the references to colour in this figure legend, the reader is referred to the web version of this article.)

the northeastern flank of the Pamir in the Tarim Basin near Oytag (Wuyitake, west China) (Fig. 2). Observed changes in detrital zircon provenance along with prograding sedimentary facies and an increase in sediment accumulation rate suggest Pamir deformation propagated outward (north–northeastward) in early to middle Miocene time.

Shifts in the isotopic composition ($\delta^{18}O$) of sedimentary carbonates have been used to constrain changes in regional topography, climate, and/or source(s) of moisture (Chamberlain and Poage, 2000; Garzione et al., 2000; Rowley et al., 2001; Kent-Corson et al., 2009). To evaluate the effects of outward growth of the Pamir plateau on regional climate, we examine the $\delta^{18}O$ values of

sedimentary carbonates in the western Tarim Basin. Our $\delta^{18}O$ results from carbonates collected in the Oytag stratigraphic section suggest that there was a reorganization of atmospheric circulation sometime during the Eocene or Oligocene, possibly related to surface uplift in the central to southeast Pamir, prior to the onset of Miocene deformation along the Pamir's northeastern flank.

2. Geologic history

Much like the Tibetan plateau, the Pamir consist of a series of terranes that accreted onto Eurasia with collisional ages that young southward (Burtman and Molnar, 1993; Matte et al., 1996; Schwab et al., 2004). The northern-most Pamir was emplaced in the late Paleozoic with subsequent stages of convergence recurring throughout the Mesozoic. Periods of continental accretion and magmatic arc development in the late Paleozoic and Mesozoic were interspersed with rift basin development and the deposition of volcaniclastics, often mantling ophiolite belts (Burtman and Molnar, 1993; Schwab et al., 2004).

Thermobarometry of lower crustal xenoliths suggest the southern Pamir plateau was substantially thickened by 50 Ma (Ducea et al., 2003; Hacker et al., 2005; Searle et al., 2010), not long after the initiation of Indo-Eurasian convergence in the western Himalaya at ~54 Ma (Rowley, 1996; Searle et al., 1997). Apatite fission-track data from the Pamir's eastern margin suggest Cenozoic shortening initiated in the middle to late Paleogene and continues through the present (Sobel and Dumitru, 1997; Yin et al., 2002). This is corroborated by (U–Th)/He cooling ages of apatite and zircon that suggest pulses of exhumation have occurred during Eocene and early to mid-Miocene time in the northern Pamir (Amidon and Hynek, 2010).

Dextral strike-slip movement in the east along the Karakorum fault and Kashgar-Yecheng transfer system accommodates up to ~280 km of internal shortening and northward translation of the Pamir relative to the Tarim Basin (Sobel and Dumitru, 1997; Murphy et al., 2000; Robinson, 2009; Cowgill, 2010). Paleomagnetic data suggest the Tajik depression off the Pamir's western margin was rotated ~52° counter-clockwise since the Miocene (Thomas et al., 1994; Burtman, 2000). Sinistral strike-slip movement along the Darvaz fault in the west may have translated the western Pamir northward relative to the Tadjik basin (Burtman and Molnar, 1993), though Thomas et al. (1994) show the Darvaz as a thrust fault. East–west extension began in the late Miocene along the Kongur Shan normal fault (Robinson et al., 2004), possibly the result of radial expansion of thickened crust under the plateau. Global Positioning System (GPS) data show the northern Pamir is currently converging with the Tian Shan at a rate of 13 ± 4 mm/a (Reigber et al., 2001).

3. Stable isotopes as a proxy for elevation and climate

We use the isotopic composition of modern water and sedimentary carbonates to infer changes in surface topography, atmospheric circulation, and climate throughout the Pamir and the western Tarim Basin. Following is a general description of the types of samples analyzed for stable isotopes in this study. The results are presented in Section 6.2.

3.1. Oxygen and hydrogen isotopes of meteoric water

Surface elevation may be estimated in regions that conform to a simple Rayleigh distillation model of air mass depletion with a definable relationship between the isotopic composition of meteoric water ($\delta^{18}O_w$, $\delta^{2}H_w$) and elevation (Gonfiantini et al., 2001; Quade et al., 2007; Rowley and Garzione, 2007). This relationship may be complicated by subcloud and surface water evaporation in arid environments (Gat, 1996). Considering that annual precipitation on the Pamir plateau is <300 mm with most sites on the eastern margin and west Tarim receiving <100 mm annually (IAEA/WMO, 2006; NOAA/NCDC, 2010), evaporation and recycling of meteoric water under low relative humidity is significant. This introduces a kinetic effect which causes more fractionation than would occur under equilibrium conditions, resulting in relatively high $\delta^{18}O_w$ and $\delta^{2}H_w$ values of meteoric water (Gat, 1996; Clark and Fritz, 1997) which may obscure the relationship between isotopic composition and elevation (Quade et al., 2007).

3.2. Oxygen isotopes of sedimentary carbonates

The isotopic composition of oxygen from carbonate ($\delta^{18}O_c$) is a reflection of the environment in which it formed. As soil carbonates mineralize, they incorporate oxygen from soil water. The absolute depth of carbonate formation in the soil is variable, depending on precipitation amount and infiltration rate, but normally is concentrated in the lower B horizon (or Bk sublayer) (Gile et al., 1966). Cemented carbonate nodules form over tens of thousands of years providing an isotopic record of soil water during this time. Because soil water often correlates with meteoric water, $\delta^{18}O_c$ values of paleosol carbonates are used to estimate the $\delta^{18}O$ of ancient meteoric water ($\delta^{18}O_w$). This correlation may break down in regions of exceptional aridity, where the annual rainfall amount is <30 mm/year (Cerling and Quade, 1993; Quade et al., 2007). In these regions soil water may reflect significantly higher $\delta^{18}O_w$ values associated with evaporative enrichment of ^{18}O. Palustrine (ponds or marshes within flood plain settings) carbonates reflect both meteoric water and groundwater across a watershed. Evaporation may cause an increase in $\delta^{18}O_w$ values, particularly in closed basins where water is lost by infiltration and evaporation (Talbot, 1990). Thus, only the most negative values are likely to reflect local rainfall compositions. Matrix cements (carbonates) from fluvial sandstones and mudstones integrate rainfall, surface water, and/or groundwater isotopic compositions (Mack et al., 2000). They precipitate during periods of waning flow and like palustrine carbonates, are subject to evaporative enrichment in arid settings. Pedogenic carbonates and shallow groundwater cements are isotopically similar (Quade and Roe, 1999). Because of their sensitivity to climate, the isotopic composition of sedimentary carbonates have been used to infer the timing of aridification of the Tarim Basin (e.g. Graham et al., 2005; Kent-Corson et al., 2009), whereby relatively high $\delta^{18}O_c$ values may be associated with an increase in evaporative conditions.

Secondary matrix cements may also precipitate from groundwater movement sometime after deposition. Care must be used when sampling as carbonates may be diagenetically altered under higher temperatures that can significantly modify the original isotopic composition, generally toward more negative values (Garzione et al., 2004).

4. Stratigraphy

Over 3700 m of Jurassic through Miocene sedimentary rocks (Fig. 3) are exposed by a major tributary to the Gez river that runs off the northeast flank of the Pamir plateau, joins the Gez river near Oytag, and continues into the Tarim Basin (Figs. 2 and DR1). The section unconformably overlies Triassic volcanics and forms the overturned western limb of a north plunging syncline (Sobel and Dumitru, 1997). The section itself is generally conformable with subvertical, overturned bedding orientations throughout.

The ages of widespread sedimentary rock formations throughout the western Tarim Basin have been loosely constrained through biostratigraphy of marine rocks using calcareous

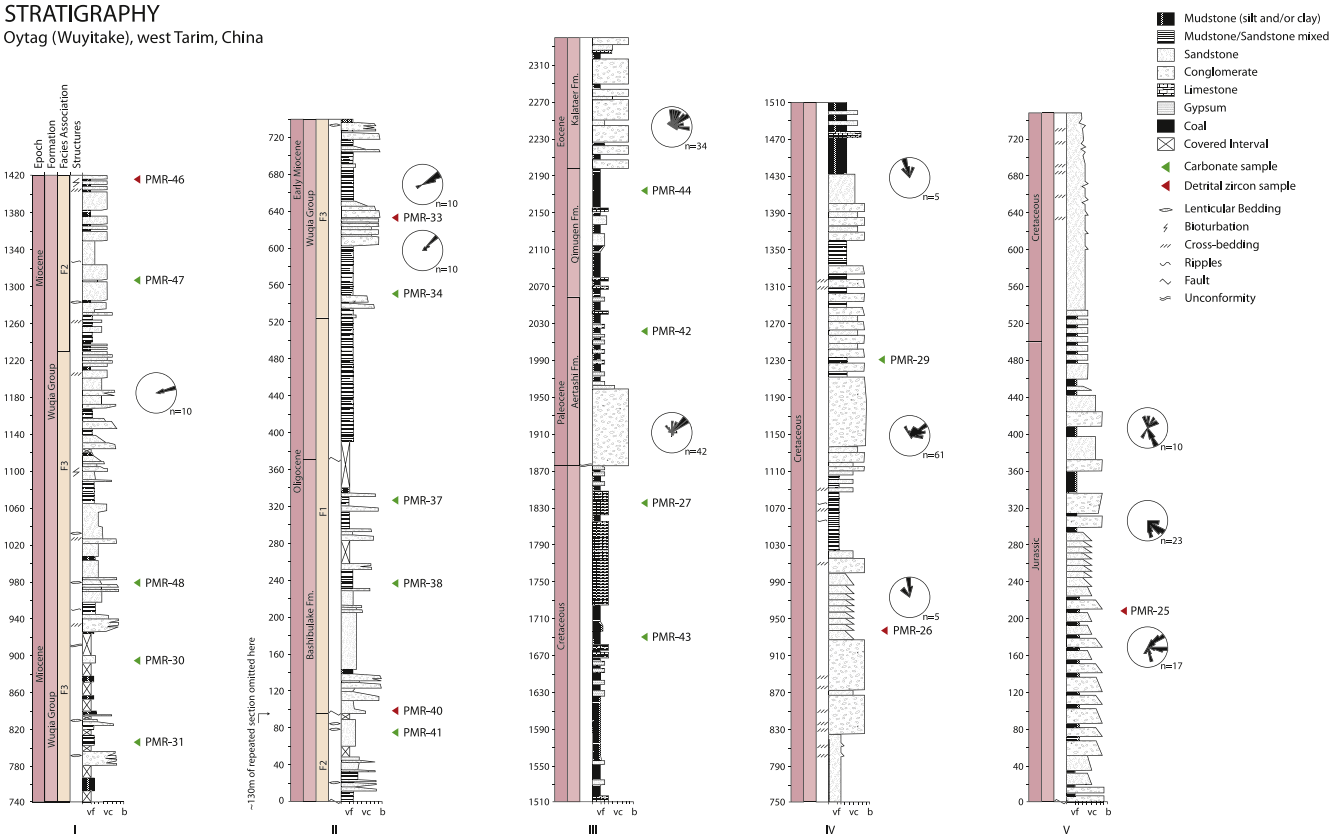

Fig. 3. Stratigraphic section of Mesozoic through Cenozoic rocks near Oytag (see Figs. 2 and DR1 for location). Mesozoic section (columns IV and V) from Sobel (1999) and Paleocene through Eocene section (column III) from Sobel (1995) (including paleocurrent data). Newly measured section shown by columns I–II. Formation names are based on lithostratigraphic units described through the Tarim Basin (Mao and Norris, 1988; Sobel, 1995; Jia et al., 2004). The Wulagen Formation is not represented which suggests a gap in measured section exists between columns II and III. Formation ages are loosely constrained through biostratigraphy of marine rocks (Hao et al., 1982; Mao and Norris, 1988; Zhong, 1989; Lan and Wei, 1995; Yang et al., 1995) and palynology of non-marine rocks (Zhou and Chen, 1990).

nannofossils, bivalves, ostracods, dinoflagellate cysts, benthic foraminifera (Hao et al., 1982; Mao and Norris, 1988; Zhong, 1989; Lan and Wei, 1995; Yang et al., 1995) and palynology of non-marine rocks (Zhou and Chen, 1990). Cenozoic strata exposed at Oytag (Wuyitake) consist of the Kashi Group, which can be subdivided into the Aertashi, Qimugen, Kalataer, Wulagen, and Bashibulake formations (Mao and Norris, 1988; Jia et al., 2004), and the younger Wuqia Group (Sobel, 1995).

Determining the presence of these formations in our measured section was done by comparing our results to stratigraphic sections from the literature for rocks at Oytag and other localities in the southwest Tarim Basin (i.e. Sobel, 1995; Yin et al., 2002; Jin et al., 2003). Correlation was supported by conspicuous markers including a prominent limestone unit at the K/T boundary, thick beds of gypsum with limestone interbeds in Paleocene and Eocene units and a fault contact/unconformity between the Bashibulake and Wuqia Group (Liu, 1990). A characteristic coarsening upward into terrestrial red-beds of the Oligo-Miocene Wuqia Group was also observed (Sobel, 1995). We know that the section at Oytag (Wuyitake) is older than ~20 Ma based on apatite fission track exhumation ages (Sobel and Dumitru, 1997) with maximum sedimentary rock ages derived from our own detrital zircon samples (Fig. 4; Table DR1).

4.1. Jurassic through early Eocene stratigraphy

Here, we include a brief summary of the Mesozoic and early Paleogene stratigraphy described and interpreted by Sobel (1999) and Sobel (1995) respectively with sections included in Fig. 3 (columns III–V). The Oytag section begins with green, organic-rich conglomerates of the Early Jurassic. The section fines upward into red and green, Middle and Late Jurassic mudstones and sandstones overlain by clast-supported conglomerate. These deposits are interpreted by Sobel (1999) to represent a braided fluvial environment proximal to its source. Paleocurrents were toward the southeast. Cretaceous strata include red fining upward sandstones with interbedded paleosols interpreted to be braided fluvial deposits (Sobel, 1999). Paleocurrents were generally toward the north and east. These deposits are overlain by gypsum-bearing mudstones followed by marine limestone in the Late Cretaceous. An unconformity marks the K-T boundary, above which ~80 m of fluvial conglomerates are deposited. This is followed by additional gypsum-bearing mudstone, limestone, and fan-delta conglomerates, suggesting a marine environment persisted into the late Paleocene and early Eocene (Sobel, 1995).

4.2. Oligocene through Miocene stratigraphy

Though our Oligocene through Miocene stratigraphic section begins approximately where Sobel's (1995) ends, the Wulagen Formation is missing which suggests a gap in measured section exists between columns II and III (Fig. 3). We have divided Oligocene through Miocene rocks (columns I and II) into three facies associations [F1–F3] using conventions from Miall (1985) and Uba et al. (2005). Facies associations (described in Section 4.2.1) are included in our stratigraphic section (Fig. 3 columns I and II) and summarized

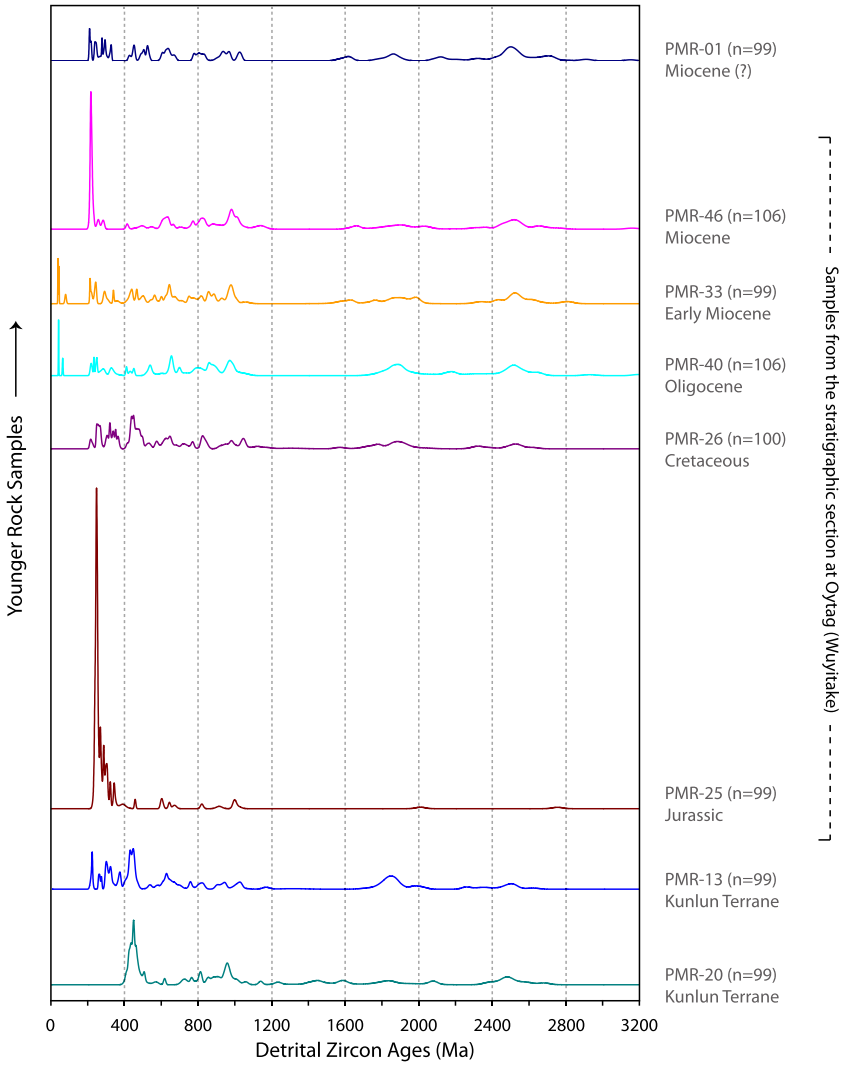

Fig. 4. Zircon age relative probability plot. Samples labeled Kunlun terrane were collected from the Muji Valley. Other samples are from the Oytag stratigraphic section (Figs. 3 and DR1). *n* = the number of zircon grains analyzed per sample.

in Table 3. Paleoflow directions were estimated using the dip and dip directions of at least 10 clasts within imbricated conglomerates.

4.2.1. Facies associations

[F1] Lenticular sandstone beds pinch out over 10s of meters and are interbedded with lenticular beds of conglomerate (2–6 m thick) that are poorly sorted, clast-supported, with sub-rounded clasts, and often show cross-bedding. Thick successions (>100 m) of red, fine-grained cross-bedded sandstone with burrows (Fig. 5A) and laterally continuous red mudstone beds are present. The [F1] facies association coincides with previous descriptions of the Bashibulake formation at Oytag (Sobel, 1995). Fossil assemblages in the Bashibulake formation suggest a neritic environment (Hao and Zeng, 1980). We interpret this to be a marginal marine lower to upper delta plain setting, consisting of sandy channel fills and mud-sized overbank deposits (Jones et al., 2001; Mack et al., 2003; Uba et al., 2005).

[F2] Brown, green, and red sandstone beds pinch out over 10s to 100s of meters. They are thickly bedded and usually horizontally laminated to massive and occasionally interbedded with sub-meter thick conglomerate that pinches out over 10s of meters. Asymmetric ripples (Fig. 5B), cross-bedding, dewatering structures, occasional pebbly layers, and scoured bases are also observed within fining upward sandstone beds. Massive, laterally continuous mudstone beds are also present but are less frequent. Sandstones are interpreted to represent channel fill deposits within a meandering river environment, while mudstones represent overbank deposits (Miall, 1996; Jones et al., 2001; Mack et al., 2003; Uba et al., 2005; Nichols and Fisher, 2007).

[F3] Conglomerate beds stack to form multistory lenticular bodies that fine upward over 10–20 meters. Pebble to cobble conglomerates are clast-supported, often imbricated, and are typically overlain by fine- to coarse-grained red and brown sandstone with floating pebbles (Fig. 5C; Fig. 5D). These successions may be separated by thick intervals (up to 60 m) of medium-grained sandstone with massive, laterally continuous red mudstone interbeds. These facies are interpreted to represent a braided fluvial fan made up of gravelly bars, sandstone bar-top deposits, and sheet-flood deposits consisting of laterally continuous mudstone (DeCelles et al., 1991; Miall, 1996; Jones et al., 2001; Nichols and Fisher, 2007). Fining upward successions likely result from waning flow associated with channel abandonment (Uba et al., 2005).

5. Analytical methods

We sampled five sedimentary rocks from our measured section at Oytag, one sedimentary rock sample that unconformably overlies the section (PMR-01), and 2 meta-sedimentary rocks from

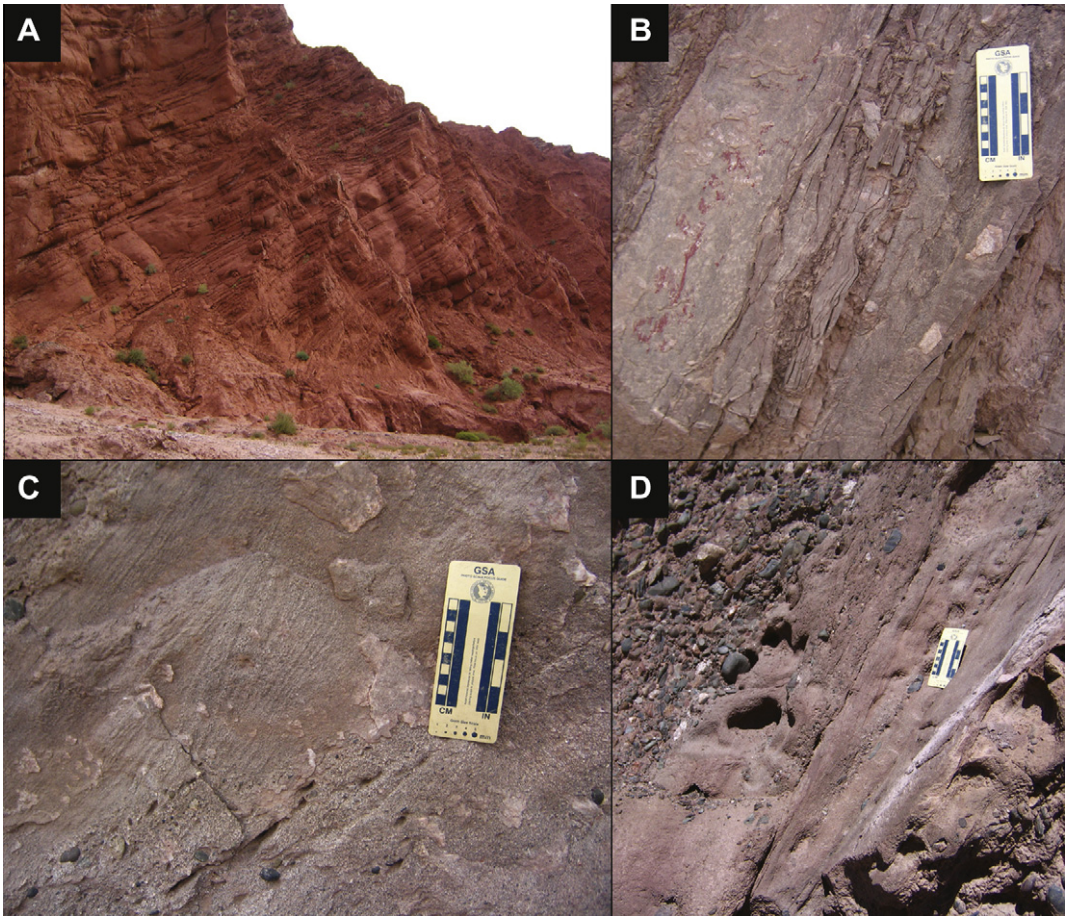

Fig. 5. Photos highlighting sedimentary structures observed in stratigraphy at Oytag (Wuyitake). In all photos, beds are overturned. (A) [F1] A thick succession (>100 m) of red, fine-grained sandstone and mudstone associated with marginal marine deposition. (B) [F2] Asymmetric ripples within the upper part of meandering river channel deposits. (C) [F3] Cross-bedding in sandstone deposited on the flanks of migrating bars in a braided fluvial environment. (D) [F3] Conglomerate overlain by cross-bedded sandstone with floating pebbles, truncated by channel scour and overlain by additional migrating bar deposits. This also represents a braided fluvial environment. (For interpretation of the references to colour in this figure legend, the reader is referred to the web version of this article.)

the Kunlun terrane on the plateau for detrital zircon analysis. We also sampled two granitic source terranes that intrude east of the section for U–Pb analysis (Fig. 4; Table DR1). In addition, 15 carbonates were sampled for stable isotope ($\delta^{18}O$) analysis (Fig. 6; Table 1). For comparison, 12 modern stream water samples were collected from small tributaries, with catchment areas <100 km^2, along the Gez River and were analyzed for their $\delta^{18}O$ and $\delta^{2}H$ values (Table 2). Though $\delta^{2}H$ results are not discussed here, we have included them for reference.

5.1. Detrital and primary zircon collection and analysis

U–Pb ages of zircons were determined by laser ablation multi-collector inductively coupled plasma mass spectrometry (LA-MC-ICPMS) at the Arizona LaserChron Center. 100 randomly selected zircon crystals from each sample were analyzed (Gehrels et al., 2008). For each analysis, the measurement error in determining $^{206}Pb/^{238}U$ and $^{206}Pb/^{204}Pb$ is ~1–2% (at 2σ level). Common Pb correction is accomplished by using the measured ^{204}Pb and assuming an initial Pb composition from Stacey and Kramers (1975). Uncertainties shown in Table DR1 are at the 1σ level, and include only measurement errors. Interpreted ages are based on $^{206}Pb/^{238}U$ for <1000 Ma grains and on $^{206}Pb/^{207}Pb$ for >1000 Ma grains. Analyses that are >30% discordant or >5% reverse discordant are not considered further. Liberal cutoffs for discordance were utilized to ensure that older ages were not preferentially excluded due to Pb loss. The resulting interpreted ages are shown on a relative age-probability diagram (Fig. 4) (from Ludwig, 2003). Plots were constructed by: (1) calculating a normal distribution for each analysis based on the reported age and uncertainty and (2) summing the probability distributions of all acceptable analyses into a single curve.

5.2. Paleosol, palustrine, and matrix carbonates

Pedogenic carbonate samples were collected from the bottom of paleosol beds, >30 cm from the top to minimize the effects of diffusion and evaporation (Cerling and Quade, 1993). All rock samples were examined under a stereoscopic microscope to identify and avoid sampling diagenetic phases of carbonate (sparite) and/or calcite veins. Samples were crushed to powder and reacted with 30% H_2O_2 for 20 min to remove organics. Analyses were carried out at the University of Rochester SIREAL laboratory on a Thermo Delta plus XP mass spectrometer in continuous-flow mode via a Thermo GasBench peripheral and a GC-PAL autosampler. Isotopic results for oxygen are reported using standard delta ($\delta^{18}O$) notation with respect to Vienna Pee Dee Belemnite (VPDB) (Fig. 6; Table 1). Three in-house standards calibrated to NBS-19 and NBS-18 were used to calculate the $\delta^{18}O_c$ of samples. The analytical precision (at 1σ) for $\delta^{18}O_c$ values is $\leqslant$±0.1‰.

5.3. Modern stream water

Gez river water was collected in the fall of 2006 along a transect from the Tarim Basin onto the Pamir plateau (Fig. 2). We followed

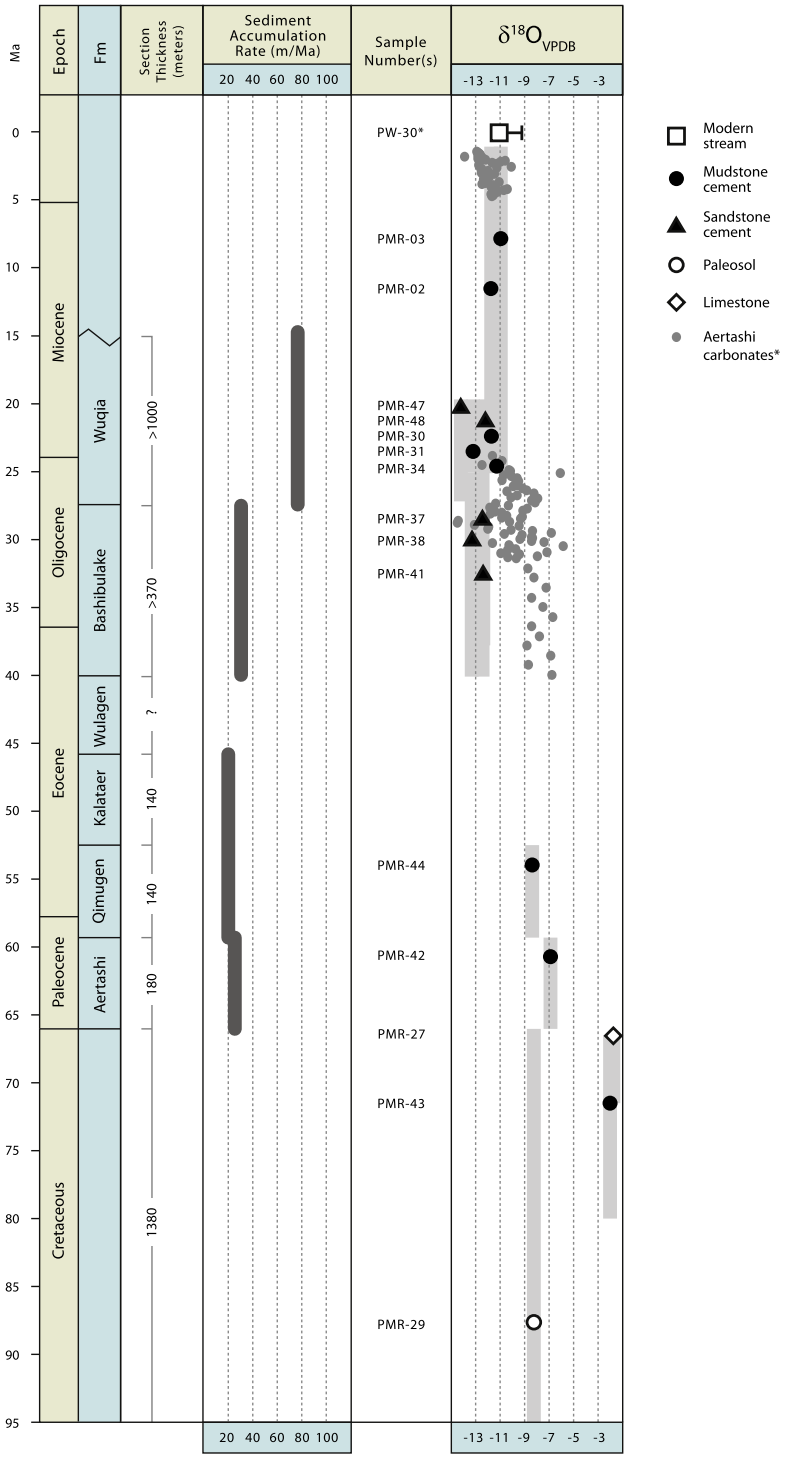

Fig. 6. $\delta^{18}O_c$ (VPDB) values from carbonate samples collected from the stratigraphic section at Oytag (Figs. 3 and DR1). PW-30 is a modern stream water sample collected from a small tributary near Oytag and converted to calcite for comparison to carbonate samples. Horizontal error bar represents the range of local, low elevation (<2500 m) surface water $\delta^{18}O_w$ values converted to calcite (Table 2). Vertical shading represents age uncertainty of carbonate samples based on formation ages (refer to Section 4 for a detailed explanation), apatite fission track exhumation ages (Sobel and Dumitru, 1997), and our own detrital zircon grain ages (Fig. 4; Table DR1). Sample ages within formations are estimated from their absolute position within the stratigraphic section. Samples PMR-02 and PMR-03 are from strata structurally above the stratigraphic section, with no upper age constraints. Aertashi carbonate data (small grey circles) from Kent-Corson et al. (2009). Sediment accumulation rates are based on measured section thickness and formation ages assuming constant sediment accumulation rates within formations.

the approach of Garzione et al. (2000) by sampling small catchments (<100 km^2) in order to minimize the elevation range and catchment area represented by each water sample. The isotopic analyses were conducted at the University of Rochester SIREAL laboratory. For oxygen analyses, ~0.5 mL of each water sample was loaded into a 12 mL Exetainer™ and flushed with a mixture of 0.3% CO_2 and UHP helium. Tubes were allowed to equilibrate for at least 18 h at ambient room temperature prior to analysis. Headspace CO_2 gas was then drawn into a Thermo Delta plus XP mass spectrometer in continuous-flow mode via a Thermo Gas Bench

Table 1
Ages[a], locality, and $\delta^{18}O$ results from carbonate samples.

Sample ID	$\delta^{18}O_{VPDB}$	Age	Sample type	Latitude	Longitude
PMR-02	−11.66	Miocene (?)	Mudstone	38.9937	75.5434
PMR-03	−10.98	Mio-Pliocene (?)	Mudstone	38.9663	75.4494
PMR-27	−1.04	Late Cretaceous	Limestone	38.9521	75.5061
PMR-29	−8.24	Cretaceous	Paleosol	38.9790	75.4780
PMR-30	−11.78	Miocene	Mudstone	38.9817	75.5215
PMR-31	−13.15	Miocene	Mudstone	38.9827	75.5194
PMR-34	−11.25	Early Miocene	Mudstone	38.9841	75.5152
PMR-37	−12.39	Oligocene	Sandstone	38.9858	75.5054
PMR-38	−13.26	Oligocene	Sandstone	38.9861	75.5037
PMR-41	−12.42	Oligocene	Sandstone	38.9868	75.4969
PMR-42	−9.40	Paleocene	Mudstone	38.9878	75.4806
PMR-43	−1.97	Cretaceous	Mudstone	38.9808	75.4814
PMR-44	−8.44	Eocene	Mudstone	38.9825	75.4881
PMR-47	−14.25	Miocene	Sandstone	38.9888	75.5384
PMR-48	−12.33	Miocene	Sandstone	38.9883	75.5347

[a] Refer to Section 4 for an explanation of age determinations.

peripheral and a GC-PAL autosampler for analysis. $\delta^{18}O$ results are calculated using internal laboratory standards calibrated to Vienna Standard Mean Ocean Water (VSMOW) and Standard Light Antarctic Precipitation (SLAP) with 1σ analytical precision $\leqslant 0.10‰$. Hydrogen analyses were run in continuous-flow mode via a Thermo Electron TC/EA peripheral. Approximately 200 nL of sample water was injected into the TC/EA during three successive injections. The reactor was set at a temperature of 1450 °C and the GC oven was set at 90 °C. The average of four injections indicates a 1σ error of <2.0‰ and values are reproducible within 4‰ in replicate analyses (Table 2).

6. Results

6.1. Zircon ages and provenance

Of eight samples analyzed, two are primary igneous rocks (PMR-08 and PMR-23) (Fig. 2). Some zircon crystals from PMR-08 are interpreted to have been affected by Pb loss given an inverse correlation between young $^{206}Pb/^{238}U$ age and higher U concentration (Fig. DR2). We have excluded crystals with U concentration >800 ppm from age calculations as lead loss results in erroneously young ages. For both igneous samples, most crystal ages are between 240 and 260 Ma, resulting in mean ages of 244 ± 4 Ma (PMR-08) and 258 ± 6 Ma (PMR-23) (Fig. DR3A and B, and Table DR1). These results are consistent with previously published U–Pb ages (245 ± 5 Ma from Robinson et al., 2004) and a bit younger than K–Ar ages (267 Ma from Chang, 1994) for the same plutons. These rocks are part of the Kunlun terrane which extends from the northern Pamir across to northeast Tibet and is made up of both Paleozoic and Triassic aged volcanic arcs (Yin and Harrison, 2000; Schwab et al., 2004).

Samples PMR-13 and PMR-20 are meta-sedimentary rocks from the Pamir hinterland (Fig. 2; Table DR1). Both samples contain detrital zircon ages clustered around ~440 Ma (Fig. 4), corresponding to older Kunlun terrane volcanics (Yin and Harrison, 2000; Schwab et al., 2004). Sample PMR-13 also has a population of grains at ~220 Ma with relatively low U/Th ratios (<4), suggesting it samples the younger volcanic arc of the Kunlun terrane as well. Sample PMR-20 does not contain any Triassic ages. Detrital grain age populations also exist at ~950 Ma, ~1.9 Ga, and ~2.5 Ga.

Five of the ten samples represent detrital zircons from the Jurassic through Miocene stratigraphic section near Oytag (Figs. 3 and DR1). The oldest of these, sample PMR-25 (Jurassic) shows a conspicuous peak at ~250 Ma that coincides with Triassic magmatism recorded in Kunlun terrane rocks (Fig. 4). Cretaceous sample PMR-26 has a more equal distribution of grain ages including both Triassic volcanics and Paleozoic meta-sedimentary rocks. An ~40 Ma peak becomes prominent in Oligocene to early Miocene samples PMR-40 and PMR-33, consistent with their designation as members of the Eocene–Oligocene Bashibulake Formation and Miocene Wuqia Group respectively (Fig. 3) (Hao and Zeng, 1980; Hao et al., 1982; Zhong, 1989; Lan and Wei, 1995). U/Th ratios of these grains are very low (<2), indicating they are primary igneous ages, not metamorphic (e.g. Hoskin and Black, 2000). No other samples from this study include zircons of this age. The source of these zircons may be the central to southeastern Pamir as U/Pb ages of shoshonitic rocks from the Muskol Antiform (Fig. 2) are late Eocene to early Oligocene in age (Ratschbacher, unpublished data). In addition, Budanov et al. (1999) report a 200 km long belt of late Eocene shoshonitic rocks dated using the palynology of interbedded sedimentary rocks trending southeast from the central Pamir near Murgab, though their exact location is not apparent from this publication. Early Eocene alkaline volcanics dated using $^{40}Ar/^{39}Ar$ (Zhang et al., 1996) that outcrop in the Tashkorgan Valley may be an extension of this belt (Fig. 2). Igneous rock grains ~39 Ma in age have also been documented in western Pamir sediments derived from the central Pamir (Lukens et al., 2009). It is also possible that the source of these ~40 Ma grains in the Oytag stratigraphic section has since been removed by erosion or is not yet documented, as high resolution mapping and geochronology in many parts of the Pamir is nonexistent. This makes interpretation of the source of these grains highly speculative.

The youngest sample from the Oytag section (PMR-46) does not contain detrital zircon grains younger than 200 Ma (Fig. 4). Rather, it shows a prominent peak at ~250 Ma, similar to the Jurassic-aged sample PMR-25. This suggests that ~40 Ma volcanic sources were cut off from the basin in association with renewed exhumation of the Kunlun terrane's Triassic volcanic arc. Sample PMR-01 was collected from strata that unconformably overlies the Oytag section (Fig. DR1), but lacks upper age limit constraints. Like PMR-46, it does not contain ~40 Ma zircon grains, but shows more distributed source terrane ages, all older than 200 Ma.

Table 2
Catchment size, locality information, and stable isotope results for tributaries along the Gez River.

Sample ID	VSMOW	$\delta^{2}H_{VSMOW}$	Elevation (m)	Catchment size (km^2)	Latitude	Longitude
PW-02	−8.08	−45.06	2088	90.7	38.8116	75.4447
PW-05	−8.80	−51.35	2399	10.6	38.7840	75.2851
PW-08	−12.47	−82.27	2595	53.7	38.7685	75.2308
PW-11	−5.33	−26.58	3053	1.2	38.7490	75.1395
PW-14	−10.94	−68.32	3249	4.8	38.7432	75.0492
PW-17	−14.29	−97.17	3454	8.4	38.9791	74.5296
PW-20	−13.02	−96.63	3486	18.2	38.9855	74.4343
PW-23	−12.23	−82.72	4075	42.5	39.1704	74.5539
PW-24	−10.99	−71.43	3363	8.3	38.8405	74.8483
PW-28	−6.70	−37.51	3179	81.9	38.7516	75.0997
PW-30	−10.00	−62.31	1969	26.0	38.8723	75.4844
PW-35	−11.57	−72.48	2704	57.1	38.9014	75.2102

6.2. Isotopic compositions of modern and paleo-waters

Of 15 carbonate samples that were analyzed for $\delta^{18}O$, eight are fluvial mudstone cements, five are fluvial sandstone cements, one is a paleosol, and one is limestone (Figs. 6 and DR1; Table 1). With the exception of PMR-43 and PMR-27, the $\delta^{18}O_c$ values of Cretaceous through early Eocene paleosol and mudstone samples are fairly consistent (average -8.7 ± 0.6‰). Of the two exceptions, PMR-27 is a marine limestone with a relatively positive $\delta^{18}O_c$ value of -1.0‰ and PMR-43 is a calcareous mudstone with a comparable $\delta^{18}O_c$ value of -2.0‰, suggesting its carbonate precipitated from marine water. A negative shift of ~4‰ occurred sometime in Eocene to Oligocene time between the deposition of samples PMR-41 and PMR-44. Although Oligo-Miocene fluvial sandstones and mudstones show more variation (average -12.6 ± 3‰), all are more negative than older samples.

Water sampled from a small tributary near the stratigraphic section (PW-30) has a $\delta^{18}O_w$ (VSMOW) value of -10‰ (Table 2). We converted this to calcite ($\delta^{18}O_c$ VPDB = -11.1‰) using the temperature-dependent fractionation equation (Kim and O'Neil, 1997) for comparison to carbonate samples. A mean annual temperature of 19 °C is assumed, which is the average temperature for relatively dry months (July, September and October) following a weakly bimodal rainy season in Kashgar (Kashi) (NOAA/NCDC, 2010). Drier months reflect the time period during which carbonates are most likely to precipitate (Breecker et al., 2009). The average $\delta^{18}O_c$ value of samples Oligocene and younger is ~1.5‰ more negative ($\delta^{18}O_c$ VPDB = -12.6 ± 3‰) than calcite calculated from modern meteoric water nearby (Fig. 6).

Two water samples collected from tributaries along the range front (PW-11 and PW-28) during a rainfall event show anomalously high $\delta^{18}O_w$ values (-5.3‰ and -6.7‰ respectively), likely reflecting runoff from that specific precipitation event as opposed to a yearly weighted average as inferred for groundwater. Excluding these two samples, stream water is generally more negative at high elevations (>3000 m) on the plateau (average = -12.3‰) when compared to lower elevation sites (<2500 m) in the Pamir foreland (average = -9.0‰), though a regression through the dataset does not produce a robust relationship between elevation and $\delta^{18}O_w$ ($R^2 = 0.48$ from Fig. 7). As discussed earlier, arid conditions throughout the region likely affect the isotopic composition of precipitation and surface water (Araguás-Araguás et al., 1998; Tian et al., 2007).

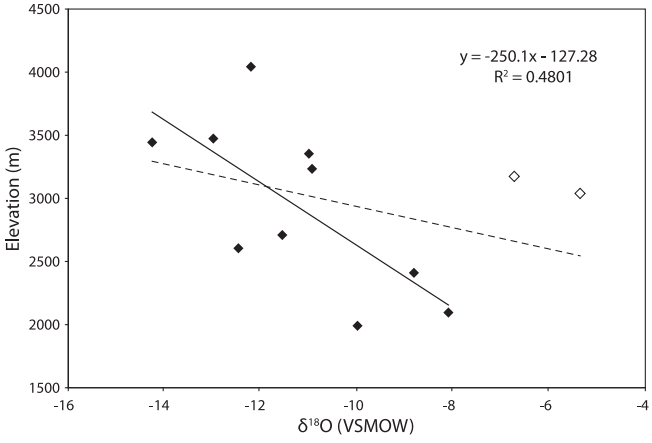

Fig. 7. Modern stream water samples from small tributaries (<100 km^2) were collected up the eastern flank of the Pamir plateau (Fig. 2 for locations) during the fall of 2006. $\delta^{18}O_w$ (VSMOW) values are plotted against sampling elevation (data from Table 2). Two samples (open diamonds) were collected along the range front while rain was observed. The regression shown by a solid line excludes these anomalously positive samples. A second regression shown by the dotted line ($R^2 = 0.132$) represents the entire dataset.

7. Discussion

7.1. Mesozoic history

The depositional setting of the Oytag basin during the Mesozoic evolved from a meandering and braided fluvial environment in the Middle Jurassic and Early Cretaceous to a marine setting in the Late Cretaceous with paleoflow directions shifting from the southeast to north–northwest respectively. The provenance of Oytag basin sediments during the Mesozoic is characterized by a transition from deposits derived almost exclusively from nearby Triassic igneous rocks during the Jurassic to sources in Paleozoic and Mesozoic terranes during the Late Cretaceous. West of Oytag, the Main Pamir Thrust (MPT) and associated fault splays place Kunlun terrane rocks over Jurassic volcaniclastics (Fig. 2). Sobel and Dumitru (1997) suggest that the Jurassic stratigraphic section was derived from these Paleozoic and Triassic volcanics based on compositional similarities and sedimentary facies which suggest proximity. This inference is partly supported by sample PMR-25 which is dominated by Triassic detrital grain ages, all with U/Th ratios <2 (Fig. 4, Table DR1). However, the near absence of Paleozoic ages in this sample suggests older volcanics currently mapped in the hanging wall of the MPT did not contribute. Whether an ancestral MPT was active at this time, facilitating exhumation of Kunlun terrane rocks, is unknown. It has been suggested that sedimentary rocks near Oytag have been translated northward since deposition, in which case their provenance may be from source terranes far to the south (Sobel and Dumitru, 1997). Erosion of Kunlun terrane rocks continued throughout the Late Cretaceous (see PMR-26 in Fig. 4), at which point the first of many marine transgressions penetrated west Tarim (Burtman and Molnar, 1993; Sobel, 1999; Burtman, 2000). The fact that Late Cretaceous marine deposition was limited to the Pamir foreland (Wang et al., 1992) suggests a greater magnitude of subsidence in western Tarim relative to the rest of the basin, possibly related to significant crustal thickening of the Pamir in the Middle Cretaceous (Robinson et al., 2004).

7.2. Cenozoic history

Results from detrital zircons suggest deformation during the Oligocene and early Miocene was focused in the Pamir hinterland with no evidence of thrusting along northeast Pamir frontal thrusts (MPT). Conspicuous ~40 Ma detrital zircon ages from igneous sources in samples PMR-40 and PMR-33 (Fig. 4) indicate that late Eocene igneous rocks, presently exposed along a volcanic belt that extends from south of Tashkorgan northwest to the Muskol antiform (Fig. 2), were eroded and deposited in the Oytag basin sometime thereafter. These results imply that the ancestral Gez river catchment reached further west than it does today. Late Eocene shoshonitic rocks may have been exhumed in the Oligocene and early Miocene by doming and normal faulting around the Muskol and Sares antiforms. This is somewhat consistent with early Miocene $^{40}Ar/^{39}Ar$ cooling ages for the Muskol antiform (Schwab et al., 2004), but predates late Miocene exhumation of the Muztaghata Massif, which is thought to be an eastern extension of the same antiform (Robinson et al., 2007). Because these ~40 Ma detrital zircon grains were deposited in the Oytag basin no later than ~20 Ma ago (Sobel and Dumitru, 1997), they may indicate that deformation of the Muskol antiform was underway by Oligocene or early Miocene time. An alternative explanation is that ~40 Ma igneous sources were exhumed by thrusting along the Tanymas, Pshart, and/or east Pamir faults (Fig. 2) which may have contained the Eocene volcanic belt in their hanging walls. It is also possible that the source of these ~40 Ma zircon grains has since been eroded.

These results preclude significant exhumation along the MPT near Oytag at this time as late Eocene igneous rocks have not been found anywhere in the MPT hanging wall (Sobel and Dumitru, 1997; Robinson et al., 2007; Cowgill, 2010). The lack of exhumation on the MPT in late Eocene time is inconsistent with the interpretation by Yin et al. (2002) that an increase in basin subsidence ~150 km southeast at Aertashi (Fig. 2) at ~37 Ma was associated with activity along frontal thrusts like the MPT.

Oytag basin provenance and stratigraphy document propagation of deformation from the central and southeastern Pamir in the Oligocene to the MPT and associated frontal thrust faults sometime in the Miocene. Convergent deformation in the southeastern Pamir had already formed thick crust (70 km) by ~50 Ma (Ducea et al., 2003; Hacker et al., 2005; Searle et al., 2010). Our results suggest that the central Pamir continued to experience exhumation throughout the Eocene as detrital zircon grains from 40 Ma igneous rocks in the central to southeast Pamir are found in Oytag sediments. In the Miocene, late Eocene zircon grains disappear from Oytag strata and Triassic ages from the Kunlun terrane become dominant again (sample PMR-46 in Fig. 4). A likely source is the hanging wall of the MPT and associated fault splays, suggesting that thrusting initiated or was reactivated in the Miocene, consistent with thermochronologic evidence (Sobel and Dumitru, 1997; Robinson et al., 2007) and a coeval change in provenance at Aertashi (Yin et al., 2002).

A basin-ward propagation of deformation during the early to mid-Miocene is corroborated by stratigraphy at Oytag which records a transition from marine to continental sedimentation from late Eocene to early Miocene time. Following the deposition of marine limestone in the Eocene, the Eocene–Oligocene Bashibulake Formation shifts to a marginal marine environment with a thick succession of mudstone and sandstone ([F1] in Fig. 3 and Table 3). The stratigraphic succession coarsens upward over ~1 km into continental braided stream and/or alluvial fan facies of the Wuqia Group [F3]. Prograding facies at Oytag coincide with a marine regression interpreted throughout the Tarim Basin (Watson et al., 1987; Bosboom et al., 2010). Paleoflow directions are consistently east-northeastward throughout the Cenozoic (Fig. 3). We interpret Oytag stratigraphy to represent a prograding succession of transverse river systems along the western margin of the Tarim Basin with sources in the Pamir, much like the modern Gez and Tashkorgan river systems (Fig. 2). Stratigraphy at Aertashi shows a similar trend from marine rocks in the middle Eocene to terrestrial fluvial and alluvial fan deposits in the Miocene (Sobel, 1995; Yin et al., 2002). Though poorly constrained, an increase in sediment accumulation rate accompanies this facies transition at Oytag from more than 30 m/Ma during the Oligocene to at least 75 m/Ma in the Miocene (Fig. 6). This may be due to increased crustal loading and exhumation along the MPT and Kashgar-Yecheng Transfer System (Fig. 2).

7.2.1. Oxygen isotopes

Oxygen isotope values ($\delta^{18}O_c$) of matrix cements from Oytag record an ~4‰ shift to more negative values during Eocene or Oligocene time (Fig. 6). Though this is roughly synchronous with a transition from marine to non-marine facies throughout western Tarim (Yin et al., 2002; Heermance et al., 2007), the observation that limestone $\delta^{18}O_c$ (PMR-27) is significantly more positive than early Paleogene matrix cements indicates that Paleogene carbonates were not precipitating from marine water. However, a marine regression could cause the source of water vapor to shift from local (Paratethys) to more distal (proto-Atlantic and/or Indian Ocean), resulting in a decrease in the $\delta^{18}O$ value of rainfall during the Oligocene. A negative shift in $\delta^{18}O_c$ values could also be caused by Paleogene surface uplift of basin-bounding ranges as inferred for sites across the southern Tarim Basin (Kent-Corson et al., 2009). This interpretation is consistent with erosion of the central to southeast Pamir inferred from 40 Ma detrital zircons in Oligo-Miocene sedimentary rocks from our stratigraphic section. It also slightly precedes the onset of aridification throughout the Tarim Basin and central Asian interior inferred from loess deposits in late Oligocene and/or early Miocene time (Guo et al., 2002; Sun et al., 2010).

The $\delta^{18}O_w$ of a small tributary near Oytag (PW-30) converted to $\delta^{18}O_c$ VPDB (−11.1‰) is ~1.5‰ more positive than $\delta^{18}O_c$ values in rocks younger than ~40 Ma (average = −12.6 ± 3‰) suggesting that $\delta^{18}O_w$ of precipitation has not varied dramatically in west Tarim since the Oligocene (Fig. 6). This implies that high relief was already established in the Pamir by this time and that deformation along the MPT, beginning in the Miocene, did not significantly affect local climate or atmospheric circulation. Unfortunately, low sample density and age uncertainty in Neogene rocks does not allow us to resolve more recent trends.

7.2.2. Regional implications

Our data suggest that central and/or southeast Pamir igneous rocks were eroded during Oligocene and early Miocene time, synchronous with widespread deformation across northern Tibet. The Altyn-Tagh fault, located along Tibet's northwest margin (Fig. 1), has been active since the latest Oligocene (Yin et al., 2002; Ritts et al., 2004; Yue et al., 2005) and Eocene deformation

Table 3
Description and interpretation of sedimentary facies (after Miall, 1985; Uba et al., 2005).

Facies association	Facies codes	Description	Interpretation
F1	Gt, Sh, Sl, Ss, St, Fb	Sandstone and mudstone (pinching out over 10s of meters) interbedded with Lenticular beds of conglomerate (2–6 m thick) that are poorly sorted, clast supported, sub-rounded, and often show cross-bedding. Thick successions (>100 m) of red, fine-grained sandstone and mudstone with some cross-beds and burrows observed	Marginal marine to lower fan delta plain environment consisting of sandy channel fills (Sl, Sh, Ss, St, Gt) and mud-sized overbank deposits (Fb). Fossil assemblages suggest a neritic environment (Hao and Zeng, 1980)
F2	Gt, Sh, Sl, Sm, Sml, Sr, St, Fl	Brown, green, and red sandstone and mudstone beds pinch out over 10s–100s of meters, both thickly bedded and laminated, with occasional ~2 m thick conglomerate interbeds (pinching out over meters). Asymmetric ripples, cross-bedding, dewatering structures, occasional pebbly layers, conspicuous calcite veins, and scoured bases observed throughout	Meandering stream environment with crevasse splay or sandy mud flows (Sm), waning-stage channel deposits (St, Sr, Sl, Sh and Fl), sand bar (St), and overbank deposits (Fl)
F3	Gm, Gt, Sh, St, Fl	Fining-upward successions (~10–20 m thick) of pebble to cobble, clast and matrix supported, often imbricated, conglomerate overlain by fine to coarse grained red and brown, often cross-bedded sandstone and mudstone with floating pebbles. Successions are often separated by thick intervals (up to 130 m) of red mudstone and medium-grained sandstone	Braided fluvial fan with gravelly bars (Gt and St), bar-top deposits (Sh and St), sheet-flood deposits (Fl), occasional mud flow and/or river flood deposits (Gm)

and exhumation in northeast Tibet has been documented along faults (Clark et al., 2010) and in basin development (Fang et al., 2003; Horton et al., 2004; Dai et al., 2006). In the Pamir, deformation propagated toward the Tarim Basin to the MPT by middle Miocene time, concurrent with deformation along the south and southeast margins of the Tarim Basin (George et al., 2001; Jolivet et al., 2001; Ritts et al., 2008) and the far northeastern edge of the Tibetan plateau (Zheng et al., 2006). Significant deformation further north throughout the Tian Shan also began in the middle Miocene (Sobel and Dumitru, 1997; Abdrakhmatov et al., 2001; Bullen et al., 2001; Heermance et al., 2007), at the same time that deformation propagated from the central and southeast Pamir toward the Tarim Basin. This suggests that stress along the flanks of the Pamir and Tibetan plateaus were quickly transferred across the relatively rigid Tarim plate to the Tian Shan. Our results do not preclude deformation in the central Pamir during this time, leaving open the possibility of synchronous Miocene deformation throughout the Pamir plateau, as is observed in Tibet (Kapp et al., 2007). However, deformation seems to have propagated northeastward from the Oligocene into the Miocene, resulting in outward growth of the Pamir plateau.

8. Conclusions

Conspicuous ~40 Ma detrital zircon grains in sedimentary rocks from the Pamir foreland indicate that deformation was focused in the central to southeast Pamir during the Oligocene to early Miocene (Fig. 4). There is no evidence of thrusting along northeast Pamir frontal thrusts (MPT) at this time as late Eocene intrusive rocks are absent from the MPT hanging wall (Sobel and Dumitru, 1997; Robinson et al., 2007; Cowgill, 2010). Oligocene to early Miocene deformation of the central Pamir was roughly coincident with an ~4‰ shift to more negative $\delta^{18}O$ values in sandstone and mudstone cements from the same stratigraphic section (Fig. 6). This shift in $\delta^{18}O$ may have been related to surface uplift of the central to southeast Pamir and other Tarim basin-bounding ranges during the Paleogene (Kent-Corson et al., 2009). It is also consistent with a marine regression at Oytag (Wuyitake) as suggested by a transition from marine rocks in the Eocene (Sobel, 1999) to terrestrial, braided fluvial deposits in the early Miocene (Fig. 3, Table 3), and prograding facies throughout the Tarim Basin (Watson et al., 1987; Bosboom et al., 2010).

In the early to middle Miocene, detrital zircons sourced from late Eocene igneous rocks disappeared from Oytag strata and Triassic detrital zircon grains eroded from Kunlun terrane rocks become prominent. This change in provenance indicates that Pamir frontal thrusts, such as the MPT, began accommodating convergence between the Pamir and the Tarim plate by early to middle Miocene time. Both provenance changes and prograding facies recorded in the Oytag stratigraphy (Fig. 3; Table 3) suggest Pamir deformation propagated toward the Tarim Basin from the Oligocene into the Miocene. This is consistent with thermochronologic data at Oytag (Sobel and Dumitru, 1997) and similar facies and compositional changes observed at Aertashi (Yin et al., 2002). Considered with Miocene crustal shortening on the northern margin of the Tibetan plateau (George et al., 2001; Jolivet et al., 2001; Zheng et al., 2006; Ritts et al., 2008) and the Tian Shan (Hendrix et al., 1994; Sobel and Dumitru, 1997; Yin et al., 1998; Abdrakhmatov et al., 2001; Bullen et al., 2001; Heermance et al., 2007), these results corroborate observations of the outward advancement of Indo-Eurasian deformation, affecting all margins of the Tarim Basin by middle Miocene time.

Acknowledgements

We are grateful to Chen Jie for help in the field. We would like to thank Alex Robinson, Ed Sobel, and Lothar Ratschberger, for insightful discussions and suggestions. We are grateful to Penny Higgins for assistance with stable isotope lab work at the University of Rochester and Alex Pullen for help running zircon samples at the University of Arizona. This work was supported by NSF Grants EAR 0506575 and EAR 0908778 to Garzione and EAR 0732436 to Gehrels (for support of the Arizona LaserChron Center) and a GSA Graduate Student Research Grant to Bershaw.

Appendix A. Supplementary data

Supplementary data associated with this article can be found, in the online version, at doi:10.1016/j.jseaes.2011.04.020.

References

Abdrakhmatov, K. et al., 2001. Onset, style, and current rate of shortening in the central Tien Shan (Kyrgyzstan). Russian Geology and Geophysics, 1502.
Amidon, W.H., Hynek, S.A., 2010. Exhumational history of the north central Pamir. Tectonics 29 (5), TC5017.
Araguás-Araguás, L., Froehlich, K., Rozanski, K., 1998. Stable isotope composition of precipitation over southeast Asia. Journal of Geophysical Research-Atmospheres 103 (D22).
Arrowsmith, J., Strecker, M., 1999. Seismotectonic range-front segmentation and mountain-belt growth in the Pamir-Alai region, Kyrgyzstan (India–Eurasia collision zone). Geological Society of America Bulletin 111 (11), 1665.
Bosboom, R.E. et al., 2010. Late Eocene sea retreat from the Tarim Basin (west China) and concomitant Asian paleoenvironmental change. Palaeogeography, Palaeoclimatology, Palaeoecology.
Breecker, D., Sharp, Z., McFadden, L., 2009. Seasonal bias in the formation and stable isotopic composition of pedogenic carbonate in modern soils from central New Mexico, USA. Geological Society of America Bulletin 121 (3–4), 630.
Bruguier, O., Lancelot, J., Malavieille, J., 1997. U–Pb dating on single detrital zircon grains from the Triassic Songpan–Ganze flysch (Central China): provenance and tectonic correlations. Earth and Planetary Science Letters 152 (1–4), 217–231.
Budanov, V., Volkova, N., Dronov, V., 1999. Petrochemistry of a rhyodacite–trachyte series in a Paleogene volcanoplutonic belt in the Southeastern Pamirs. Russian Geology and Geophysics 40 (5), 648–654.
Bullen, M., Burbank, D., Garver, J., Abdrakhmatov, K., 2001. Late Cenozoic tectonic evolution of the northwestern Tien Shan: new age estimates for the initiation of mountain building. Geological Society of America Bulletin 113 (12), 1544.
Burtman, V., 2000. Cenozoic crustal shortening between the Pamir and Tien Shan and a reconstruction of the Pamir–Tien Shan transition zone for the Cretaceous and Palaeogene. Tectonophysics 319 (2), 69–92.
Burtman, V., Molnar, P., 1993. Geological and Geophysical Evidence for Deep Subduction of Continental Crust Beneath the Pamir. Geological Society of America.
Cerling, T.E., Quade, J., 1993. Stable carbon and oxygen isotopes in soil carbonates. Geophysical Monograph – American Geophysical Union 78, 217.
Chamberlain, C., Poage, M., 2000. Reconstructing the paleotopography of mountain belts from the isotopic composition of authigenic minerals. Geology 28 (2), 115.
Chang, C., 1994. Tectonic evolution of western Tibetan Plateau. In: Proceedings of the International Symposium on the Karakorum and Kunlun Mountains. China Meteorol., Beijing, pp. 11–22.
Clark, I., Fritz, P., 1997. Environmental Isotopes in Hydrogeology. CRC Press/Lewis Publishers.
Clark, M.K., Farley, K.A., Zheng, D., Wang, Z., Duvall, A.R., 2010. Early Cenozoic faulting of the northern Tibetan Plateau margin from apatite (U–Th)/He ages. Earth and Planetary Science Letters 296 (1–2), 78–88.
Coutand, I. et al., 2002. Late Cenozoic tectonic development of the intramontane Alai Valley, (Pamir-Tien Shan region, central Asia): an example of intracontinental deformation due to the Indo-Eurasia collision. Tectonics 21 (6), 1053.
Cowgill, E., 2010. Cenozoic right-slip faulting along the eastern margin of the Pamir salient, northwestern China. Geological Society of America Bulletin 122 (1–2), 145–161.
Dai, S. et al., 2006. Magnetostratigraphy of Cenozoic sediments from the Xining Basin: tectonic implications for the northeastern Tibetan Plateau. Journal of Geophysical Research 111 (B11), B11102.
DeCelles, P. et al., 1991. Kinematic history of a foreland uplift from Paleocene synorogenic conglomerate, Beartooth Range, Wyoming and Montana. Geological Society of America Bulletin 61 (4).
Ducea, M. et al., 2003. Building the Pamirs: the view from the underside. Geology 31 (10), 849.
Fang, X., Garzione, C., Van der Voo, R., Li, J., Fan, M., 2003. Flexural subsidence by 29 Ma on the NE edge of Tibet from the magnetostratigraphy of Linxia Basin, China. Earth and Planetary Science Letters 210 (3–4), 545–560.
Garzione, C.N., Quade, J., DeCelles, P.G., English, N.B., 2000. Predicting paleoelevation of Tibet and the Himalaya from d18O vs. altitude gradients in meteoric water across the Nepal Himalaya. Earth and Planetary Science Letters 183 (1–2), 215–229.

Garzione, C., Dettman, D., Horton, B., 2004. Carbonate oxygen isotope paleoaltimetry: evaluating the effect of diagenesis on paleoelevation estimates for the Tibetan plateau. Palaeogeography, Palaeoclimatology, Palaeoecology 212 (1–2), 119–140.

Gat, J., 1996. Oxygen and hydrogen isotopes in the hydrologic cycle. Annual Review of Earth and Planetary Sciences 24 (1), 225–262.

Gehrels, G., Dickinson, W., 1995. Detrital zircon provenance of Cambrian to Triassic miogeoclinal and eugeoclinal strata in Nevada. American Journal or Science 295, 18–48.

Gehrels, G., Valencia, V., Ruiz, J., 2008. Enhanced precision, accuracy, efficiency, and spatial resolution of U–Pb ages by laser ablation–multicollector–inductively coupled plasma–mass spectrometry. Geochemistry Geophysics Geosystems 9 (3), Q03017.

George, A., Marshallsea, S., Wyrwoll, K., Jie, C., Yanchou, L., 2001. Miocene cooling in the northern Qilian Shan, northeastern margin of the Tibetan Plateau, revealed by apatite fission-track and vitrinite-reflectance analysis. Geology 29 (10), 939.

Gile, L.H., Peterson, F.F., Grossman, R.B., 1966. Morphological and genetic sequences of carbonate accumulation in desert soils. Soil Science 101 (5), 347–360.

Gonfiantini, R., Roche, M.A., Olivry, J.C., Fontes, J.C., Zuppi, G.M., 2001. The altitude effect on the isotopic composition of tropical rains. Chemical Geology 181 (1–4), 147–167.

Graham, S. et al., 2005. Stable isotope records of Cenozoic climate and topography, Tibetan Plateau and Tarim Basin. American Journal of Science 305 (2), 101.

Guo, Z. et al., 2002. Onset of Asian desertification by 22 Myr ago inferred from loess deposits in China. Nature 416 (6877), 159–163.

Hacker, B. et al., 2005. Near-ultrahigh pressure processing of continental crust: Miocene crustal xenoliths from the Pamir. Journal of Petrology 46 (8), 1661–1688.

Hao, Y., Zeng, X., 1980. Early Tertiary Foraminifera from the Kashi basin of Xinjiang. Acta Palaeontologica Sinica 19, 152–169.

Hao, Y., Zeng, X., Qiu, S., He, X., 1982. Miocene foraminifera of Tarim Basin, Xinjiang, and their geological significance. Bulletin of Chinese Academy of Geological Sciences 4, 70–79.

Heermance, R., Chen, J., Burbank, D., Wang, C., 2007. Chronology and tectonic controls of Late Tertiary deposition in the southwestern Tian Shan foreland, NW China. Basin Research 19 (4), 599.

Hendrix, M., Dumitru, T., Graham, S., 1994. Late Oligocene-early Miocene unroofing in the Chinese Tian Shan: an early effect of the India–Asia collision. Geology 22 (6), 487.

Horton, B. et al., 2004. Mesozoic–Cenozoic evolution of the Xining-Minhe and Dangchang basins, northeastern Tibetan Plateau: magnetostratigraphic and biostratigraphic results. Journal of Geophysical Research 109 (B04402), 1–15.

Hoskin, P., Black, L., 2000. Metamorphic zircon formation by solid-state recrystallization of protolith igneous zircon. Journal of Metamorphic Geology 18 (4), 423–440.

IAEA/WMO, 2006. Global Network of Isotopes in Precipitation. <http://isohis.iaea.org>.

Ireland, T., Flöttmann, T., Fanning, C., Gibson, G., Preiss, W., 1998. Development of the early Paleozoic Pacific margin of Gondwana from detrital-zircon ages across the Delamerian orogen. Geology 26 (3), 243.

Jia, C., Zhang, S., Wu, S., 2004. Stratigraphy of the Tarim basin and Adjacent Areas, vol. 1. Science Press, Beijing.

Jin, X., Wang, J., Chen, B., Ren, L., 2003. Cenozoic depositional sequences in the piedmont of the west Kunlun and their paleogeographic and tectonic implications. Journal of Asian Earth Sciences 21 (7), 755–765.

Jolivet, M. et al., 2001. Mesozoic and Cenozoic tectonics of the northern edge of the Tibetan plateau: fission-track constraints. Tectonophysics 343 (1–2), 111–134.

Jones, S., Frostick, L., Astin, T., 2001. Braided stream and flood plain architecture: the Rio Vero Formation, Spanish Pyrenees. Sedimentary Geology 139 (3–4), 229–260.

Kapp, P., DeCelles, P., Gehrels, G., Heizler, M., Ding, L., 2007. Geological records of the Lhasa–Qiangtang and Indo-Asian collisions in the Nima area of central Tibet. Geological Society of America Bulletin 119 (7–8), 917.

Kent-Corson, M. et al., 2009. Stable isotopic constraints on the tectonic, topographic, and climatic evolution of the northern margin of the Tibetan Plateau. Earth and Planetary Science Letters 282 (1–4), 158–166.

Kim, S., O'Neil, J., 1997. Equilibrium and nonequilibrium oxygen isotope effects in synthetic carbonates. Geochimica et Cosmochimica Acta 61 (16), 3461–3475.

Lan, X., Wei, J., 1995. Late Cretaceous–Early Tertiary Marine Bivalve Fauna from the Western Tarim Basin. Chinese Science Publishing House, Beijing.

Liu, W., 1990. Contact relationship between Upper and Lower Tertiary and age ownership of Wuqia Group in the southwest depression of Tarim Basin. Xinjiang Petroleum Geology 11, 20–24.

Ludwig, K., 2003. User's manual for Isoplot 3.00: a geochronological toolkit for Microsoft Excel. Berkeley Geochronology Center Special Publication 4, 70.

Lukens, C., Carrapa, B., Schoenbohm, L., Singer, B., Jicha, B., 2009. Tectono-thermal Evolution of the Western Pamir Mountains, Using $^{40}Ar/^{39}Ar$ Thermochronology on Modern River Sands, p. 2099.

Mack, G., Cole, D., Treviño, L., 2000. The distribution and discrimination of shallow, authigenic carbonate in the Pliocene–Pleistocene Palomas Basin, southern Rio Grande rift. Geological Society of America Bulletin 112 (5), 643.

Mack, G., Leeder, M., Perez-Arlucea, M., Bailey, B., 2003. Early Permian silt-bed fluvial sedimentation in the Orogrande basin of the Ancestral Rocky Mountains, New Mexico, USA. Sedimentary Geology 160 (1–3), 159–178.

Mao, S., Norris, G., 1988. Late Cretaceous – Early Tertiary Dinoflagellates and Acritarchs from the Kashi Area, Tarim Basin, Xinjiang Province, China. Life Science Contributions, vol. 150. Royal Ontario Museum, p. 93.

Matte, P. et al., 1996. Tectonics of Western Tibet, between the Tarim and the Indus. Earth and Planetary Science Letters 142 (3), 311–316.

Miall, A., 1985. Architectural-element analysis: a new method of facies analysis applied to fluvial deposits. Earth Science Reviews 22, 261–308.

Miall, A., 1996. The Geology of Fluvial Deposits. Sedimentary Facies, Basin Analysis, and Petroleum Geology. Springer, Berlin, p. 582.

Murphy, M. et al., 2000. Southward propagation of the Karakoram fault system, southwest Tibet: timing and magnitude of slip. Geology 28, 451.

Nichols, G., Fisher, J., 2007. Processes, facies and architecture of fluvial distributary system deposits. Sedimentary Geology 195 (1–2), 75–90.

NOAA/NCDC, 2010. National Oceanic and Atmospheric Administration and National Climatic Data Center, Asheville, North Carolina. <http://www.ncdc.noaa.gov>.

Quade, J., Roe, L., 1999. The stable-isotope composition of early ground-water cements from sandstone in paleoecological reconstruction. Journal of Sedimentary Research 69 (3), 667.

Quade, J., Garzione, C., Eiler, J., 2007. Paleoelevation reconstruction using pedogenic carbonates. Reviews in Mineralogy and Geochemistry 66 (1), 53.

Reigber, C. et al., 2001. New space geodetic constraints on the distribution of deformation in Central Asia. Earth and Planetary Science Letters 191 (1–2), 157–165.

Ritts, B., Yue, Y., Graham, S., 2004. Oligocene Miocene Tectonics and sedimentation along the Altyn Tagh Fault, Northern Tibetan Plateau: analysis of the Xorkol, Subei, and Aksay Basins. The Journal of Geology 112, 207–229.

Ritts, B. et al., 2008. From sea level to high elevation in 15 million years: uplift history of the northern Tibetan Plateau margin in the Altun Shan. American Journal of Science 308 (5), 657.

Robinson, A., 2009. Geologic offsets across the northern Karakorum fault: implications for its role and terrane correlations in the western Himalayan–Tibetan orogen. Earth and Planetary Science Letters 279 (1–2), 123–130.

Robinson, A. et al., 2004. Tectonic evolution of the northeastern Pamir: constraints from the northern portion of the Cenozoic Kongur Shan extensional system, western China. Bulletin of the Geological Society of America 116 (7–8), 953–973.

Robinson, A. et al., 2007. Cenozoic evolution of the eastern Pamir: implications for strain-accommodation mechanisms at the western end of the Himalayan–Tibetan orogen. Geological Society of America Bulletin 119 (7–8), 882.

Rowley, D., 1996. Age of initiation of collision between India and Asia: a review of stratigraphic data. Earth and Planetary Science Letters 145 (1–4), 1–13.

Rowley, D.B., Garzione, C.N., 2007. Stable isotope-based paleoaltimetry. Annual Review of Earth and Planetary Sciences 35 (1), 463–508.

Rowley, D.B., Pierrehumbert, R.T., Currie, B.S., 2001. A new approach to stable isotope-based paleoaltimetry: implications for paleoaltimetry and paleohypsometry of the High Himalaya since the Late Miocene. Earth and Planetary Science Letters 188 (1–2), 253–268.

Schwab, M. et al., 2004. Assembly of the Pamirs: age and origin of magmatic belts from the southern Tien Shan to the southern Pamirs and their relation to Tibet. Tectonics 23 (4).

Searle, M., Corfield, R., Stephenson, B., McCarron, J., 1997. Structure of the North Indian continental margin in the Ladakh–Zanskar Himalayas: implications for the timing of obduction of the Spontang ophiolite, India–Asia collision and deformation events in the Himalaya. Geological Magazine 134 (03), 297–316.

Searle, M. et al., 2010. Anatomy, age and evolution of a collisional mountain belt: the Baltoro granite batholith and Karakoram Metamorphic Complex, Pakistani Karakoram. Journal of Geological Society 167 (1), 183.

Sobel, E., 1995. Basin Analysis and Apatite Fission-track Thermochronology of the Jurassic–Paleogene Southwest Tarim Basin, Northwest China. Ph. D. Thesis, Stanford, California, Stanford University.

Sobel, E.R., 1999. Basin analysis of the Jurassic-Lower Cretaceous Southwest Tarim Basin, Northwest China. Geological Society of America Bulletin 111 (5), 709–724.

Sobel, E., Dumitru, T., 1997. Thrusting and exhumation around the margins of the western Tarim basin during the India–Asia collision. Journal of Geophysical Research 102, 5043–5064.

Stacey, J., Kramers, J., 1975. Approximation of terrestrial lead isotope evolution by a two-stage model. Earth and Planetary Science Letters 26, 207.

Sun, J. et al., 2010. Late Oligocene–Miocene mid-latitude aridification and wind patterns in the Asian interior. Geology 38 (6), 515.

Talbot, M.R., 1990. A review of the palaeohydrological interpretation of carbon and oxygen isotopic ratios in primary lacustrine carbonates. Chemical Geology 80, 261–279.

Thomas, J. et al., 1994. Paleomagnetic evidence for Cenozoic block rotations in the Tadjik depression (Central Asia). Journal of Geophysical Research-Solid Earth 99 (B8).

Tian, L. et al., 2007. Stable isotopic variations in west China: a consideration of moisture sources. Journal of Geophysical Research 112, D10112.

Uba, C.E., Heubeck, C., Hulka, C., 2005. Facies analysis and basin architecture of the Neogene Subandean synorogenic wedge, southern Bolivia. Sedimentary Geology 180 (3–4), 91–123.

Wang, Q., Nishidai, T., Coward, M., 1992. The Tarim Basin, NW China: formation and aspects of petroleum geology. Journal of Petroleum Geology 15 (1), 5–34.

Watson, M., Hayward, A., Parkinson, D., Zhang, Z., 1987. Plate tectonic history, basin development and petroleum source rock deposition on shore China. Marine and Petroleum Geology 4 (3), 205–225.

Yang, H., Jiang, X., Lin, S., 1995. Late Cretaceous – Early Tertiary Ostracod Fauna from Western Tarim Basin. South Xinjiang, China, Beijing, p. 173.
Yin, A., Harrison, T., 2000. Geologic evolution of the Himalayan–Tibetan orogen. Annual Review of Earth and Planetary Sciences 28 (1), 211–280.
Yin, A. et al., 1998. Late Cenozoic tectonic evolution of the southern Chinese Tian Shan. Tectonics 17 (1).
Yin, A. et al., 2002. Tectonic history of the Altyn Tagh fault system in northern Tibet inferred from Cenozoic sedimentation. Geological Society of America Bulletin 114 (10), 1257.
Yue, Y., Graham, S., Ritts, B., Wooden, J., 2005. Detrital zircon provenance evidence for large-scale extrusion along the Altyn Tagh fault. Tectonophysics 406 (3–4), 165–178.
Zhang, Y., Xie, Y., Xu, R., Vidal, P., Arnaud, N., 1996. Geochemistry of Granitoid Rocks. Geological Evolution of the Karakorum and Kunlun Mountains. Seismological Press, Beijing, pp. 94–136.
Zheng, D. et al., 2006. Rapid exhumation at 8 Ma on the Liupan Shan thrust fault from apatite fission-track thermochronology: implications for growth of the northeastern Tibetan Plateau margin. Earth and Planetary Science Letters 248, 198–208.
Zhong, S.-l., 1989. Significance of Calcareous Nannofossil Assemblage from Bashibulake Formation (Paleogene) in Western Tarim Basin, Xinjiang. Acta Palaeontologica Sinica, 1.
Zhou, Z., Chen, P., 1990. Biostratigraphy and Geologic Evolution: Petroleum Geology of Tarim Basin. Science Press, Beijing, p. 366.